Technical Note

Highly Efficient Respiratory Motion Compensated Free-Breathing Coronary MRA Using Golden-Step Cartesian Acquisition

Claudia Prieto, PhD,[1,2]* Mariya Doneva, PhD,[3] Muhammad Usman, PhD,[1] Markus Henningsson, PhD,[1] Gerald Greil, MD,[1] Tobias Schaeffter, PhD,[1] and Rene M. Botnar, PhD[1]

Purpose: To develop an efficient 3D affine respiratory motion compensation framework for Cartesian whole-heart coronary magnetic resonance angiography (MRA).

Materials and Methods: The proposed method achieves 100% scan efficiency by estimating the affine respiratory motion from the data itself and correcting the acquired data in the reconstruction process. For this, a golden-step Cartesian sampling with spiral profile ordering was performed to enable reconstruction of respiratory resolved images at any breathing position and with different respiratory window size. Affine motion parameters were estimated from image-based registration of 3D undersampled respiratory resolved images reconstructed with iterative SENSE and motion correction was performed directly in the reconstruction using a multiple-coils generalized matrix formulation method. This approach was tested on healthy volunteers and compared against a conventional diaphragmatic navigator-gated acquisition using quantitative and qualitative image quality assessment.

Results: The proposed approach achieved 47 ± 12% and 59 ± 6% vessel sharpness for the right (RCA) and left (LAD) coronary arteries, respectively. Also, good quality visual scores of 2.4 ± 0.74 and 2.44 ± 0.86 were observed for the RCA and LAD (scores from 0, no to 4, excellent coronary vessel delineation). A not statically significant difference ($P = 0.05$) was found between the proposed method and an 8-mm navigator-gated and tracked scan, although scan efficiency increased from 61 ± 10% to 100%.

Conclusion: We demonstrate the feasibility of a new 3D affine respiratory motion correction technique for Cartesian whole-heart CMRA that achieves 100% scan efficiency and therefore a predictable acquisition time. This approach yields image quality comparable to that of an 8-mm navigator-gated acquisition with lower scan efficiency. Further evaluation of this technique in patients is now warranted to determine its clinical use.

Key Words: coronary MRI; image navigator; respiratory motion correction; undersampling
J. Magn. Reson. Imaging 2014;00:000–000.

DESPITE ONGOING PROGRESS and developments in magnetic resonance (MR) acquisition and reconstruction technology, respiratory motion remains a major problem in coronary MR angiography (CMRA). The currently used methods typically employ 1D navigator echoes to estimate the respiratory signal from the foot-head (FH) translational motion of the diaphragm, which is employed to gate and correct data acquisition of the heart (1). Respiratory gating is used to acquire MR data only when the respiratory signal coincides with a predefined acceptance window, preferably end-expiration, while all other data are being rejected. Residual motion within the gating window or bin is usually corrected using a predefined tracking factor of 0.6 that accounts for the relationship between respiratory-induced diaphragmatic and cardiac motion (2). This approach has been shown to considerably reduce motion artifacts when small gating windows are employed; however, it leads to prolonged scan times since only a fraction of the acquired data is accepted for reconstruction (referred to as scan efficiency). Moreover, in subjects with highly irregular breathing patterns, drift in respiratory motion can lead to scan abortions due to low scan efficiency. Another drawback of the navigator-gated approach is

[1]King's College London, Division of Imaging Sciences and Biomedical Engineering, London, UK.
[2]Pontificia Universidad Católica de Chile, Escuela de Ingeniería, Santiago, Chile.
[3]Philips Research Europe, Hamburg Tomographic Imaging Department, Hamburg, Germany.
The last two authors contributed equally to this work.
Contract grant sponsor: Institute for Health Research (NIHR) Biomedical Research Centre at Guy's and St Thomas' NHS Foundation Trust and King's College London. The views expressed are those of the authors and not necessarily those of the NHS, the NIHR or the Department of Health. C. Prieto acknowledges financial support from FONDECYT 11110053.
*Address reprint requests to: C.P., Division of Imaging Sciences and Biomedical Engineering, Rayne Institute, 4th Floor, Lambeth Wing, St Thomas' Hospital, London, SE1 7EH, UK.
E-mail: claudia.prieto@kcl.ac.uk
Received December 18, 2013; Accepted January 31, 2014.
DOI 10.1002/jmri.24602
View this article online at wileyonlinelibrary.com.

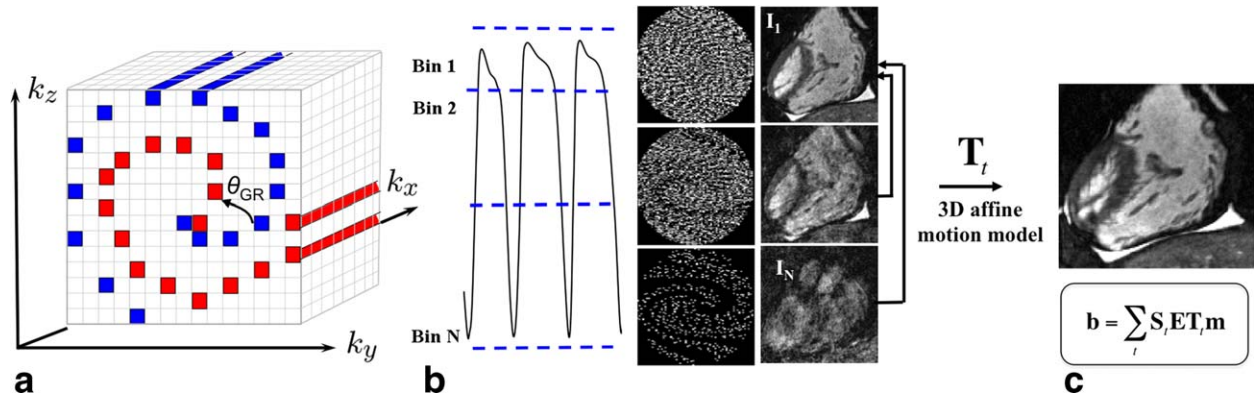

Figure 1. Proposed approach. **a:** Image acquisition is performed using a golden-step Cartesian trajectory with spiral profile ordering, where the angular step between two consecutive spiral interleaves is given by the golden ratio. **b:** Acquired data is binned into different respiratory positions according to their position in the respiratory signal given by a 1D navigator echo; the undersampled data at each bin is then reconstructed using iterative SENSE to obtain respiratory-resolved undersampled images that can be registered to a common respiratory position. **c:** 3D affine motion parameters T_t estimated from image-based registration are incorporated directly in the reconstruction process using a matrix description of general motion correction. [Color figure can be viewed in the online issue, which is available at wileyonlinelibrary.com.]

the use of an oversimplified and patient-independent model for motion correction that accounts for FH translational motion only. Studies have shown that, especially for large or no gating windows, 3D affine transformations are needed to accurately model the motion of the heart throughout the respiratory cycle (3,4).

Several approaches have been proposed to overcome some of these problems, including subject-specific tracking factors to improve motion correction (5,6), self-gating techniques to simplify acquisition and directly estimate the respiratory induced cardiac motion from the acquired data (7–9), and image-based navigators to eliminate the need of respiratory motion models and allow separation of static tissues from the moving heart (10–15). Most of these approaches correct respiratory motion in a beat-to-beat fashion; however, they are typically limited to 1D, 2D, or 3D translational motion only. To account for more complex and 3D motion, "respiratory binning" techniques have been recently proposed (16–19). With this approach the respiratory signal is divided into several states of the breathing cycle or "bins" and afterwards corrected to a reference position using the motion estimated from low-resolution images. These methods achieve 100% scan efficiency and therefore reduce the acquisition time. A 3D CMRA radial acquisition has been used previously (16,19) to estimate the respiratory motion between bins from the data itself by reconstructing low-resolution images at each respiratory bin. The drawbacks to this approach are that radial trajectories intrinsically have a lower signal-to-noise ratio (SNR) compared with Cartesian trajectories (20,21), epicardial fat recovery may impair image quality for long acquisition windows, as radial trajectories repeatedly sample the center of *k*-space (22), and prolonged reconstruction time. Similar approaches using respiratory binning have been implemented for Cartesian sampling (17,18); however, they require the acquisition of dedicated low-resolution images in addition to the CMRA data, which may result in a time delay between motion sensing and the actual CMRA acquisition.

In this work, we propose a new 3D respiratory binning motion correction approach for Cartesian whole-heart CMRA which does not require the acquisition of additional data for motion estimation. This approach achieves 100% scan efficiency by estimating the motion from the data itself and correcting the acquired data directly in the reconstruction process. This is accomplished by using a golden-step Cartesian acquisition with spiral profile order (G-CASPR) to enable reconstruction of respiratory resolved images at any breathing position and with different respiratory window size. Affine motion parameters are estimated from image-based registration of 3D undersampled respiratory resolved images reconstructed with iterative sensitivity encoding (SENSE) (23) and motion correction is performed directly in the reconstruction using a multiple-coils generalized matrix formulation method (24). This approach was tested on healthy volunteers and compared against a conventional diaphragmatic navigator-gated acquisition to assess the feasibility of the proposed framework.

MATERIALS AND METHODS

The proposed approach can be divided into three steps, as illustrated in Fig. 1. In the first step, image acquisition is performed using a Cartesian trajectory allowing reconstruction of respiratory resolved undersampled images. Second, image-based registration is performed to estimate the affine tissue deformation between the image at the most common respiratory position (typically end-expiration) and all remaining respiratory images. Finally, the estimated motion is used to correct the acquired data in the reconstruction process using a matrix description of general motion correction (24). The following sections describe all three steps in further detail, as well as the experiments performed to validate this approach.

Image Acquisition

To allow reconstruction of multiple 3D images at different respiratory positions throughout the entire breathing cycle, a quasi-uniform *k*-space distribution should be ensured in each respiratory window. However, *k*-space distribution in each window is difficult to predict since breathing patterns vary in each subject and for each scan. To overcome this problem, data are acquired using G-CASPR, an extension of (25). G-CASPR samples the phase-encoding plane following approximate spiral interleaves on the Cartesian grid. The angular step between two consecutive spiral interleaves is given by the golden ratio $\varphi = 0.618$ (Fig. 1a). More details of the sampling implementation follow. This trajectory ensures quasi-uniform *k*-space sampling at any breathing position and for any respiratory window, independently of the breathing pattern due the golden angle step properties (26).

The G-CASPR sampling pattern defines a temporal ordering of phase-encoding lines on a Cartesian grid (ky-kz) that resemble approximate spirals. The segmentation of the Cartesian grid in approximate spirals is performed by the following procedure: 1) First, the total number of phase-encoding lines in an elliptical ky-kz plane is adjusted to an integer multiple of N × M, where N is the number of phase-encoding lines for each spiral interleaf and M is the number of spiral interleaves; 2) then the elliptical ky-kz plane is segmented in N concentric elliptical rings and the phase-encoding lines within each ring are sorted according to increasing angle; 3) the spiral interleaves are defined to perform a full 360° turn from the center of *k*-space to the periphery. This is achieved by splitting each elliptical ring in N angular segments and defining the spiral interleaves by picking the phase-encoding lines in the sorted order starting from the central to the outermost ring and moving to the next angular segment with each successive ring. For example, the first spiral is obtained with the samples in (ring 1, angular segment 1) – (ring 2, angular segment 2) – … – (ring N, angular segment N), whereas the second spiral samples (ring 1, angular segment 2) – (ring 2, angular segment 3) – … – (ring N, angular segment 1). This leads to spiral interleaves sorted according to increasing angle from 0 to 360°; and 4) finally, the spiral interleaves are temporally ordered according to a golden ratio permutation. In order to do this each spiral interleaf is labeled by its central angle in angular steps of $2\pi/M$, where M is the number of spiral interleaves. The golden ratio permutation of the corresponding angles is determined by successively selecting the angle closest to $2\pi\gamma n$ wrapped to the interval $[0, 2\pi]$, where $\gamma = 2/(1+\sqrt{5})$ is the golden ratio and $n = 1, 2, \ldots$ is the iteration number. After selecting a certain angle, it is removed from the list such that after M iterations all angles from the list are selected.

Steps 1–3 are shown in a schematic example in Fig. 2. Let's consider 21 spiral interleaves and 9 samples per interleaf. First, the elliptical region of 21 × 9 samples is divided in 9 concentric elliptical rings (regions in red – green – blue – orange – cyan – pink – yellow – brown and gray in Fig. 2). Then the 21 samples per ring are sorted according to increasing angles (order indicated by numbers of the color of each concentric elliptical region in Fig. 2). Finally, the spiral interleaves are defined to perform a full 360° turn from the center of *k*-space to the periphery by selecting the phase-encoding lines in the sorted order starting from the central to the outermost ring and moving to the next angular segment with each successive ring. In the example in Fig. 2, the order of the first spiral will be: 1 red – 2 green – 3 blue – 4 orange – 5 cyan – 6 pink – 7 yellow – 8 brown – 9 gray.

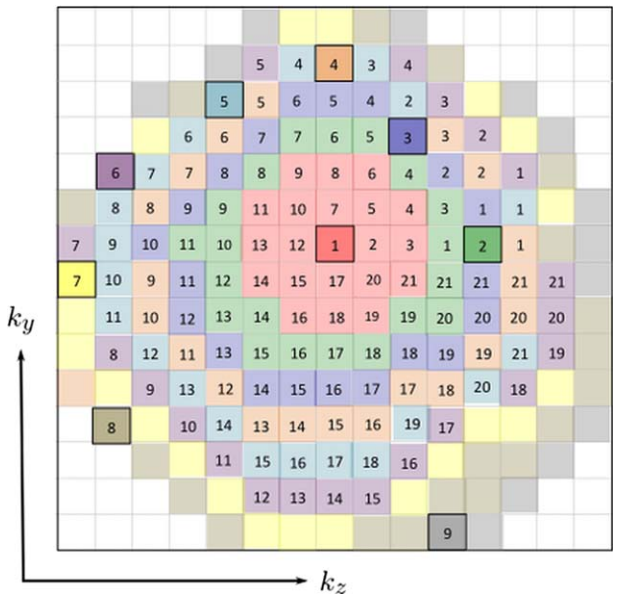

Figure 2. Schematic example of steps (a–c) in G-CASPR trajectory design. First, the elliptical region is divided in concentric elliptical rings (rings in red – green – blue – orange – cyan – pink – yellow – brown and gray). Then the samples per ring are sorted according to increasing angles (order indicated by numbers of the color of each concentric elliptical region in the figure). Finally, the spiral interleaves are defined to perform a full 360° turn from the center of *k*-space to the periphery by selecting the phase-encoding lines in the sorted order starting from the central to the outermost ring and moving to the next angular segment with each successive ring. In this example the order of the first spiral will be: 1 red – 2 green – 3 blue – 4 orange – 5 cyan – 6 pink – 7 yellow – 8 brown – 9 gray.

Motion Estimation

The acquired data were retrospectively assigned to five respiratory bins according to their position in the breathing cycle (given by the 1D diaphragmatic navigator signal), with bin 1 at end-expiration and bin 5 at end-inspiration. Since data assigned to each window are undersampled, iterative SENSE was performed to reconstruct the five undersampled respiratory resolved images. The corresponding undersampling factor varies for each respiratory position according to the breathing cycle, being lower for the most common respiratory position (ie, end-expiration) and higher for the remaining breathing stages. Similar to previous

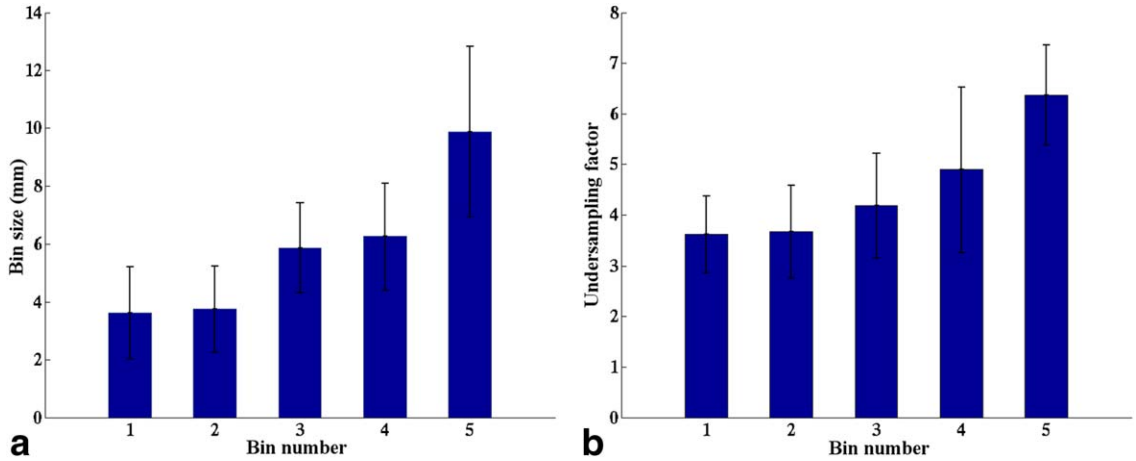

Figure 3. Results for data binning strategy: (**a**) average bin size at each respiratory position (bin 1: end-expiration, bin 5: end-inspiration) for all eight volunteers; (**b**) undersampling factor at each respiratory position for all eight volunteers. The large average width for bin 5 was due to the presence of outliers and the lower frequency of samples at this respiratory position. [Color figure can be viewed in the online issue, which is available at wileyonlinelibrary.com.]

studies (27,28), an adaptive binning was performed to ensure a maximum acceleration factor of 8 for all respiratory resolved images using a 32-channel coil. This is possible due to the flexibility of the golden-step approach. The size of each bin was initially defined uniformly according to the amplitude of the respiratory cycle. Subsequently, the width was increased in a sliding window fashion (leading to overlapping bins) for those bins that yield to acceleration factors higher than 8 to ensure enough data for reconstruction.

Before undersampled reconstruction, intra-bin translational motion correction was performed in the FH (readout) direction using the diaphragmatic navigator signal and a tracking factor of 0.6 to minimize motion within large-size bins. *K*-space data in each bin was corrected to the average navigator position within that bin using a phase modulation.

Subsequently, the undersampled reconstructed intra-bin corrected respiratory resolved images were registered to the most common respiratory position (usually end-expiration) to yield 3D affine motion parameters (Fig. 1b). The 3D affine transformation is a 12-parameter model that describes translation, rotation, shear, and scaling in three dimensions. Image-based registration was performed in a region of interest around the heart using an intensity based image registration (29).

Image Reconstruction

The estimated 3D affine motion parameters were incorporated directly in the reconstruction using a matrix description of general motion correction (24). This is an exact formulation for the effect of any motion (rigid, affine, or nonrigid) during acquisition of *k*-space. Considering $\mathbf{m}$ as the motion-free object to be reconstructed, the motion corrupted *k*-space data $\mathbf{b}$ is given by:

$$\mathbf{b} = \sum_t \mathbf{S}_t \mathbf{E} \mathbf{T}_t \mathbf{m}$$

where $\mathbf{T}_t$ (t = 1,...,5) is a motion matrix that warps the pixels in the reference image $\mathbf{m}$ to the remaining respiratory positions, $\mathbf{E}$ the encoding matrix, consisting of coil sensitivities and Fourier transform, and $\mathbf{S}_t$ is the sampling operator that selects the k-samples acquired at the t^{th} respiratory position. This image reconstruction problem is solved iteratively using a linear conjugate gradient method (30).

In Vivo Experiments

Eight healthy subjects (31.8 ± 6.8 years, all men) were scanned on a 1.5T MRI scanner (Philips Achieva, Best, The Netherlands) using a 32-channel cardiac receiver coil. Written informed consent was obtained from all volunteers in accordance with the ethical rules of our institution. 3D segmented balanced steady-state free precession (SSFP) fully sampled G-CASPR acquisitions were performed under free breathing without a gating window. Relevant scan parameters include: field of view (FOV) = 288 × 288 × 100 mm, resolution = 1 × 1 × 2 mm, TR/TE/flip angle = 4.5msec/2.2msec/70°, T_2 preparation pulse (TE = 50 msec), fat saturation prepulse (SPIR), subject-specific mid-diastolic trigger delay, subject-specific acquisition window ~100–120 msec (20–24 profiles per cardiac cycle), one spiral-like interleaf per R-R interval and coronal orientation. A fully sampled 8-mm navigator gate and track (tracking factor of 0.6) acquisition was performed at end-expiration with the same trajectory (G-CASPR) and identical imaging parameters for comparison purposes. For a fair comparison, the order of acquisition of the two sequences was randomized.

The ungated acquisition was reconstructed both with the proposed motion correction and without motion correction. Five undersampled respiratory resolved images covering the complete breathing cycle were reconstructed for each volunteer with the proposed method. Undersampling factors for each bin were typically between 3× and 8× depending on the respiratory position and breathing pattern. The image of the bin with the lowest undersampling factor (usually end-expiration) was considered as reference and the images at the remaining respiratory positions were registered

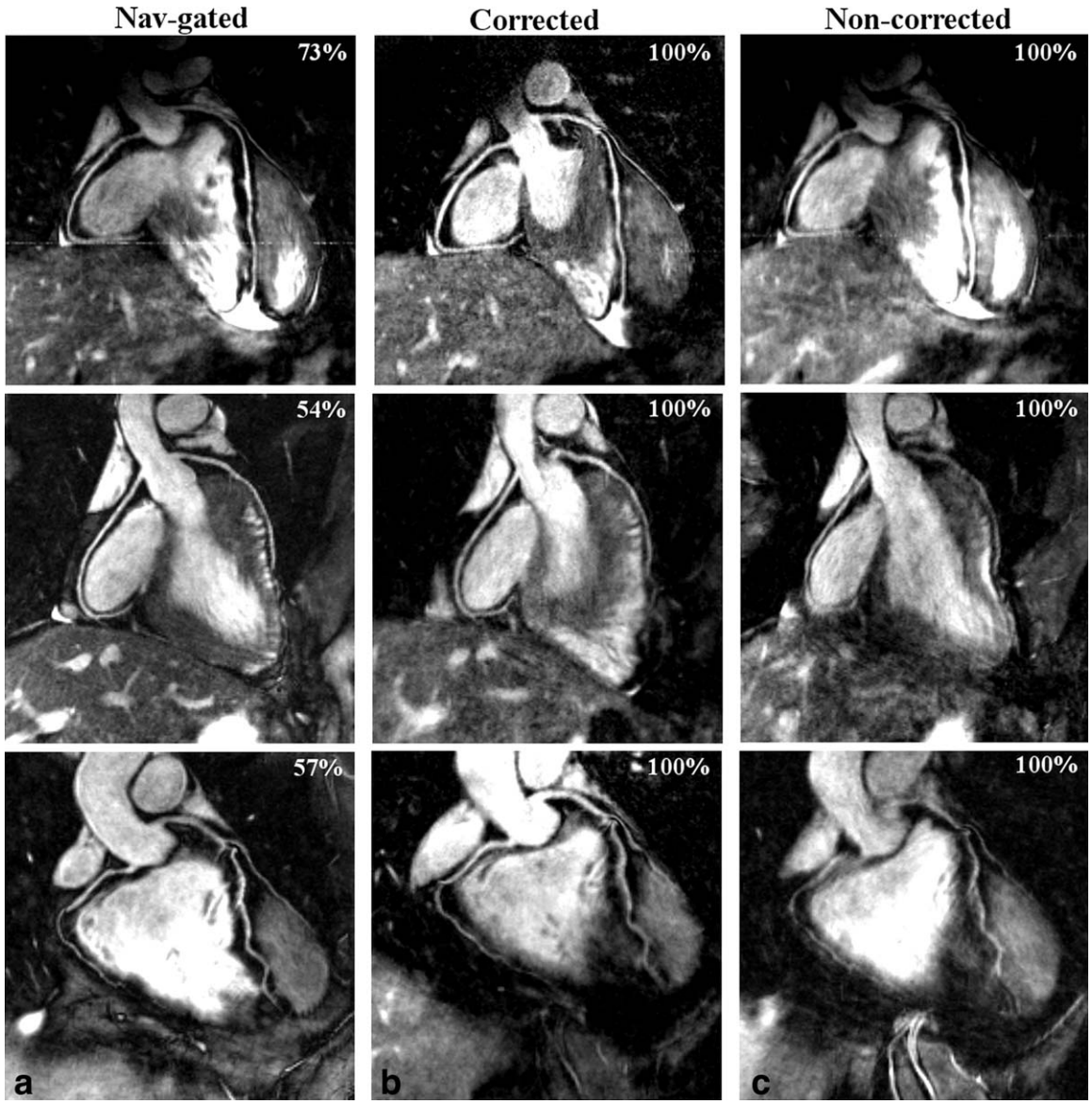

Figure 4. Reformatted images along the RCA and LAD artery from three healthy volunteers. **a:** Navigator-gated and tracked acquisition with 8-mm navigator window and 0.6 scaling factor (nav-gated). **b:** Ungated acquisition reconstructed with proposed motion correction approach (corrected). **c:** Ungated acquisition with no motion correction (noncorrected). Good depiction of RCA and LAD is observed with both nav-gated and corrected approaches; however, blurring can be observed in the LAD and distal RCA when no motion correction is performed. Scan efficiency is indicated in the superior right-hand side of each image. A radiofrequency artifact was present during acquisition of volunteer 1 (top row).

to that bin using an affine motion model in a region of interest around the heart. All reconstructions were performed offline with MatLab (MathWorks, Natick, MA) on a 12-Core PC with 196GB memory.

The three reconstructions: 1) no respiratory gating with proposed motion correction (corrected), 2) no respiratory gating without motion correction (noncorrected), and 3) 8-mm navigator-gated and slice tracking (nav-gated) were reformatted to visualize the right coronary artery (RCA) and the left anterior descending artery (LAD), using dedicated software (31). Reconstruction results were compared in terms of visualized RCA and LAD vessel lengths and sharpness. Vessel sharpness values were normalized relative to the signal intensity of the centerline of each vessel; therefore, 100% sharpness refers to a maximum signal intensity change at the vessel edge.

Qualitative image scoring was also performed by two independent, experienced observers (M.H. and G.G. with 5 and 15 years of experience, respectively, in cardiac MRI) who were blinded to the technique employed. The three reconstructed images (ie, corrected, noncorrected, and nav-gated) were presented simultaneously and next to each other to the observers. The order of these three images was randomly modified for the different volunteers. A visual score was given for the RCA, LAD, and overall image using a five-point scale: 0, no; 1, poor; 2, fair; 3, good; and 4, excellent coronary vessel delineation.

The differences of the quantitative measurements for the three reconstructions were tested with a paired *t*-test with a P value of 0.05 considered statistically significant. A Wilcoxon signed-rank test was used to

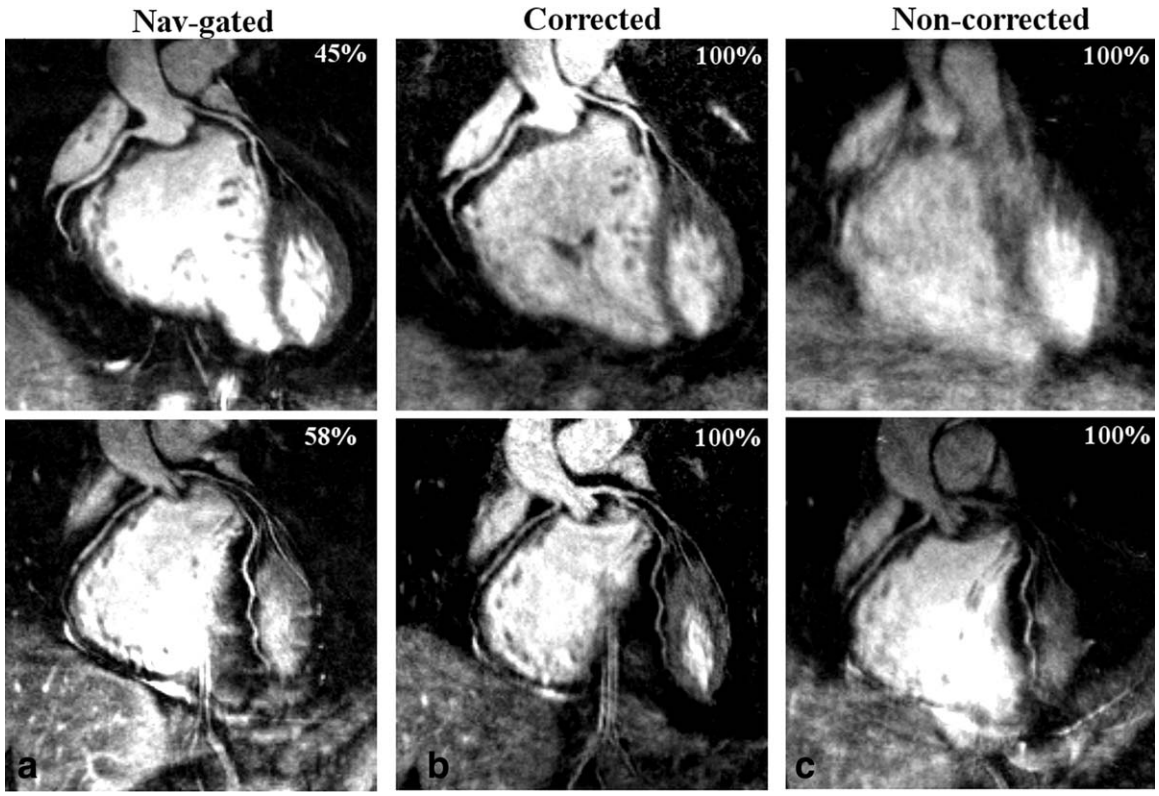

Figure 5. Reformatted images along the RCA and LAD artery from two healthy volunteers where coronary artery visualization is obscured if no motion correction is performed. **a:** Navigator-gated and tracked acquisition with 8-mm navigator window and 0.6 scaling factor (nav-gated). **b:** Ungated acquisition reconstructed with proposed motion correction approach (corrected). **c:** Ungated acquisition with no motion correction (noncorrected). The proposed motion correction approach shows significantly improved image quality in comparison with the noncorrect approach; however, slightly decreased quality in comparison with the nav-gated acquisition.

test the qualitative measurements for statistical significance difference with a P value of 0.05.

RESULTS

Scans were completed successfully in all subjects. The average scan time with the proposed motion correction technique was 8.49 ± 1.00 minutes with 100% scan efficiency. The average scan time for the navigator-gated and tracked acquisition was 14.14 ± 2.94 minutes with 61 ± 10% scan efficiency. Therefore, the acquisition was approximately two times faster with the proposed approach. The results of the data binning strategy required by the proposed technique are presented in Fig. 3, which shows the average size and undersampling factor resulting for each bin across all subjects. The large average width for bin 5 was due to the presence of extreme respiratory positions (outliers) and the lower frequency of samples at that respiratory position. The bin size was reduced from 9.87 ± 2.94 mm to 8.12 ± 2.85 mm when outliers were discarded, but also reducing scan efficiency slightly from 100% to 99.66 ± 0.26%. In the present study outliers were not discarded. Reconstruction results for the 8-mm navigator-gated and slice tracking acquisition (nav-gated), the ungated and corrected proposed approach (corrected), and ungated without motion correction (noncorrected) reformatted images are shown in Fig. 4a–c, respectively, for three particular volunteers. Good depiction of the RCA and LAD is observed with the nav-gated and proposed approaches. However, motion blurring is observed in the noncorrected images with the same acquisition time as the proposed technique. In several cases (3 out of 8) the blurring was substantial enough to significantly obscure the visualization of the RCA and LAD, as can be seen in Fig. 5 for two particular volunteers. In these cases the proposed approach shows significantly improved image quality in comparison with the noncorrected approach; however, with slightly decreased quality in comparison with the navigator-gated and tracked acquisition. Analysis of quality measurements for all reconstructed datasets is shown in Fig. 6 including RCA and LAD vessel length and thickness as well as the visual scores. Both RCA and LAD vessel sharpness and lengths show no significant difference with the proposed motion correction in comparison with the navigator-gated approach. A significant increment in LAD vessel sharpness and RCA vessel length was observed with the proposed approach in comparison with the noncorrected one. The visual scores for RCA, LAD, and overall image quality were not significantly different for the proposed approach in comparison with the gated acquisition, whereas all of them were significantly lower with no motion correction.

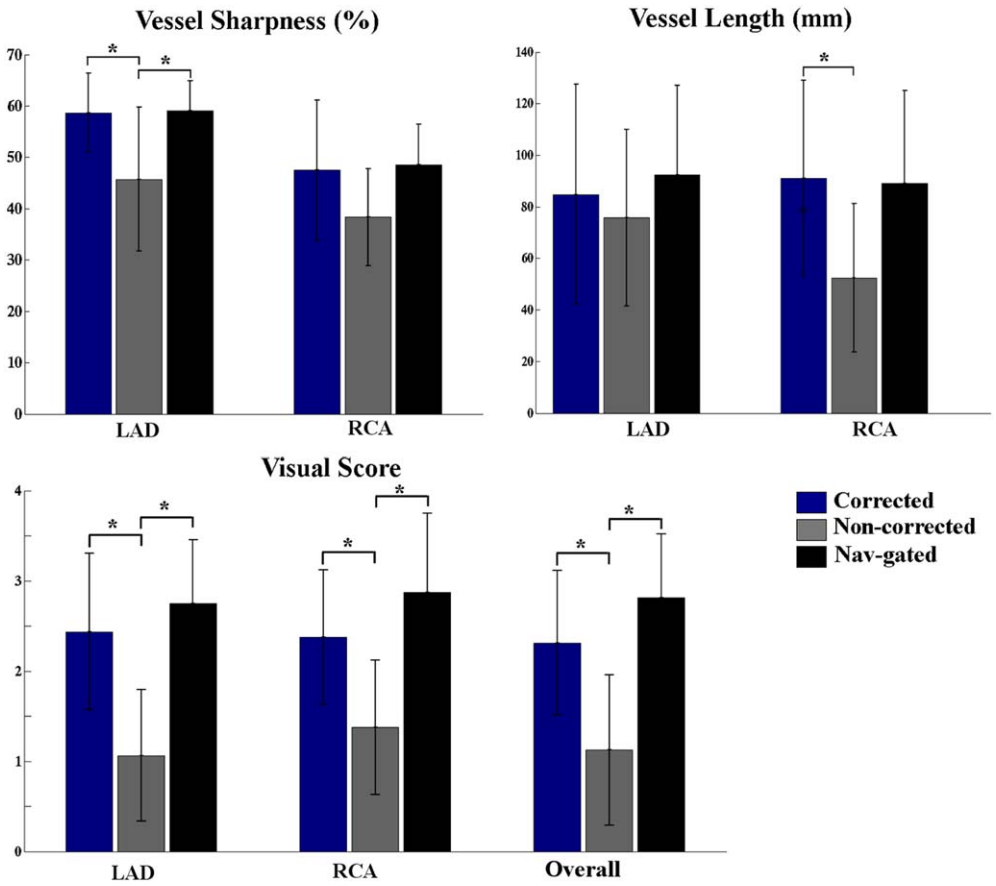

Figure 6. Quantitative (vessel sharpness and length) and qualitative (visual score) results from healthy volunteer study. *Statistically significant differences ($P < 0.05$). [Color figure can be viewed in the online issue, which is available at wileyonlinelibrary.com.]

The proposed approach was implemented in MatLab and the results in a total processing time of ~40 minutes per dataset using a 12-core CPU.

DISCUSSION

A novel approach for 3D affine respiratory motion corrected Cartesian whole-heart coronary MRA has been proposed. This method takes advantage of the reconstruction flexibility of G-CASPR to reconstruct undersampled images at different respiratory bins, which can be used for motion estimation and correction. The proposed method performs 1D translational intra-bin and 3D affine inter-bin motion correction. The results show that the proposed approach achieves good image quality, for both RCA and LAD. A not statically significant difference was found between the proposed method and a diaphragmatic navigator acquisition with 8-mm gating window and a slice tracking factor of 0.6. Visual scores show a slight bias towards the nav-gated reconstruction that may have been produced because the three reconstructions were shown simultaneously and next to each other to the observers. This scoring procedure provides a reference to the observers but also may incite them to rank the images from the highest to the lowest quality. On average, the proposed method reduces the acquisition time by 1.7 in comparison with the navigator-gated approach and yields predictable scan duration.

In the current study, five respiratory bins were employed since this resulted in a reasonable trade-off between bin size and the amount of data within each bin. To minimize errors in the motion estimation due to residual aliasing artifacts, a maximum undersampling factor of 8 was enforced for each bin, as has been shown for similar trajectories, increasing the bin size in a sliding window fashion when this condition was not satisfied. This resulted in a reasonable average bin size of 4.87 mm for bins 1 to 4 and an average bin size of 9.87 mm for bin 5 when outliers were not discarded. To minimize intra-bin motion for large bin sizes, a 1D translational motion correction was performed before calculation of the affine parameters and undersampled reconstruction. Good results were achieved with this strategy for a coronary artery whole-heart protocol using a 32-channel coil.

Compared with other Cartesian techniques (17,18) this method does not require the acquisition of additional dedicated navigator images for motion estimation since respiratory resolved images are reconstructed from the CMRA data itself, therefore reducing the delay between motion sensing and CMRA acquisition. Compared with the radial approach proposed by Bhat et al and Pang et al (16,19), this method estimates the motion from undersampled SENSE reconstructed images with the same spatial resolution as the underlying CMRA data; achieves higher signal-to-noise ratio (SNR) due to the Cartesian sampling strategy; and does not require any gridding operation during the reconstruction.

The proposed approach was implemented in MatLab and results in a total processing time of ~40 minutes

per dataset using a 12-core CPU. However, this is a suboptimal implementation and the total reconstruction could be considerably reduced by using a processing unit implementation (32).

In this work a generalized matrix formulation approach was used to correct for affine motion directly in the reconstruction process. This matrix formulation can account for any kind of motion and therefore the proposed approach can also be used to correct for nonrigid deformations that may be caused by respiratory drifts. This may improve image quality for those subjects with more complex motion of the heart. The reconstruction time is increased when nonrigid motion correction is performed and therefore was not considered in this study.

The current study used a fully sampled CMRA acquisition to ensure a reasonable undersampling factor for each respiratory bin. Further reduction of the acquisition time can be achieved by undersampling the underlying CMRA data provided sufficient image quality for motion estimation is achieved at each respiratory bin. This can be accomplished by reconstructing all respiratory bins simultaneously using k-t techniques (33) to exploit redundancy between different breathing positions. The use of the generalized matrix formulation approach allows reconstructing the undersampled CMRA using information from the coil sensitivities to estimate the nonacquired data during the motion corrected reconstruction process.

One limitation of this work is that respiratory binning was performed retrospectively based on a 1D diaphragmatic navigator signal. However, the proposed trajectory can be modified for self-gating by acquiring the *k*-space center for each segment. This will be investigated in future work to allow intra-bin 1D translational motion correction without the need of a motion model.

In conclusion, we have proposed a new 3D affine respiratory motion correction technique for Cartesian whole-heart coronary MRA that achieves 100% scan efficiency and therefore a predictable acquisition time. This technique estimates the affine respiratory motion from the data itself and corrects the acquired data in the reconstruction process. We showed that the proposed method yields image quality comparable to that of an 8-mm navigator-gated longer scan time acquisition and that it outperforms the noncorrected acquisition with the same acquisition time. Further evaluation of this technique in patients is now warranted to determine its clinical use.

REFERENCES

1. Wang Y, Rossman PJ, Grimm RC, Riederer SJ, Ehman RL. Navigator-echo-based real-time respiratory gating and triggering for reduction of respiration effects in three-dimensional coronary MR angiography. Radiology 1996;198:55–60.
2. Wang Y, Riederer SJ, Ehman RL. Respiratory motion of the heart: kinematics and the implications for the spatial resolution in coronary imaging. Magn Reson Med 1995;33:713–719.
3. Manke D, Nehrke K, Bornert P, Rosch P, Dossel O. Respiratory motion in coronary magnetic resonance angiography: a comparison of different motion models. J Magn Reson Imaging 2002;15:661–671.
4. Shechter G, Ozturk C, Resar JR, McVeigh ER. Respiratory motion of the heart from free breathing coronary angiograms. IEEE Trans Med Imaging 2004;23:1046–1056.
5. Taylor AM, Keegan J, Jhooti P, Firmin DN, Pennell DJ. Calculation of a subject-specific adaptive motion-correction factor for improved real-time navigator echo-gated magnetic resonance coronary angiography. J Cardiovasc Magn Reson 1999;1:131–138.
6. Moghari MH, Hu P, Kissinger KV, et al. Subject-specific estimation of respiratory navigator tracking factor for free-breathing cardiovascular MR. Magn Reson Med 2012;67:1665–1672.
7. Stehning C, Bornert P, Nehrke K, Eggers H, Stuber M. Free-breathing whole-heart coronary MRA with 3D radial SSFP and self-navigated image reconstruction. Magn Reson Med 2005;54:476–480.
8. Piccini D, Littmann A, Nielles-Vallespin S, Zenge MO. Respiratory self-navigation for whole-heart bright-blood coronary MRI: methods for robust isolation and automatic segmentation of the blood pool. Magn Reson Med 2012;68:571–579.
9. Lai P, Bi X, Jerecic R, Li D. A respiratory self-gating technique with 3D-translation compensation for free-breathing whole-heart coronary MRA. Magn Reson Med 2009;62:731–738.
10. Keegan J, Gatehouse PD, Yang GZ, Firmin DN. Non-model-based correction of respiratory motion using beat-to-beat 3D spiral fat-selective imaging. J Magn Reson Imaging 2007;26:624–629.
11. Scott AD, Keegan J, Firmin DN. Beat-to-beat respiratory motion correction with near 100% efficiency: a quantitative assessment using high-resolution coronary artery imaging. Magn Reson Imaging 2011;29:568–578.
12. Henningsson M, Koken P, Stehning C, Razavi R, Prieto C, Botnar RM. Whole-heart coronary MR angiography with 2D self-navigated image reconstruction. Magn Reson Med 2012;67:437–445.
13. Henningsson M, Smink J, Razavi R, Botnar RM. Prospective respiratory motion correction for coronary MR angiography using a 2D image navigator. Magn Reson Med 2013;69:486–494.
14. Kawaji K, Spincemaille P, Nguyen TD, et al. Direct coronary motion extraction from a 2D fat image navigator for prospectively gated coronary MR angiography. Magn Reson Med 2013 [Epub ahead of print].
15. Wu HH, Gurney PT, Hu BS, Nishimura DG, McConnell MV. Free-breathing multiphase whole-heart coronary MR angiography using image-based navigators and three-dimensional cones imaging. Magn Reson Med 2013;69:1083–1093.
16. Bhat H, Ge L, Nielles-Vallespin S, Zuehlsdorff S, Li D. 3D radial sampling and 3D affine transform-based respiratory motion correction technique for free-breathing whole-heart coronary MRA with 100% imaging efficiency. Magn Reson Med 2011;65:1269–1277.
17. Schmidt JF, Buehrer M, Boesiger P, Kozerke S. Nonrigid retrospective respiratory motion correction in whole-heart coronary MRA. Magn Reson Med 2011;66:1541–1549.
18. Henningsson M, Prieto C, Chiribiri A, Vaillant G, Razavi R, Botnar RM. Whole-heart coronary MRA with 3D affine motion correction using 3D image-based navigation. Magn Reson Med 2014;71:173–181.
19. Pang J, Bhat H, Sharif B, et al. Whole-heart coronary MRA with 100% respiratory gating efficiency: self-navigated three-dimensional retrospective image-based motion correction (TRIM). Magn Reson Med 2014;71:67–74.
20. Lauzon ML, Rutt BK. Effects of polar sampling in k-space. Magn Reson Med 1996;36:940–949.
21. Pipe JG, Duerk JL. Analytical resolution and noise characteristics of linearly reconstructed magnetic resonance data with arbitrary k-space sampling. Magn Reson Med 1995;34:170–178.
22. Prieto C, Botnar RM, Schaeffter T.Improving fat suppression in radial coronary MRA using a weighted golden ratio acquisition. In: Proc 19th Annual Meeting ISMRM, Montreal; 2011. p 1268.
23. Pruessmann KP, Weiger M, Bornert P, Boesiger P. Advances in sensitivity encoding with arbitrary k-space trajectories. Magn Reson Med 2001;46:638–651.
24. Batchelor PG, Atkinson D, Irarrazaval P, Hill DL, Hajnal J, Larkman D. Matrix description of general motion correction applied to multishot images. Magn Reson Med 2005;54:1273–1280.
25. Doneva M, Stehning C, Nehrke K, Bornert P.Improving scan efficiency of respiratory gated imaging using compressed sensing

with 3D Cartesian golden angle sampling. In: Proc 19th Annual Meeting ISMRM, Montreal; 2011. p 641.
26. Winkelmann S, Schaeffter T, Koehler T, Eggers H, Doessel O. An optimal radial profile order based on the Golden Ratio for time-resolved MRI. IEEE Trans Med Imaging 2007;26:68–76.
27. Buerger C, Clough RE, King AP, Schaeffter T, Prieto C. Nonrigid motion modeling of the liver from 3-D undersampled self-gated golden-radial phase encoded MRI. IEEE Trans Med Imaging 2012;31: 805–815.
28. Usman M, Atkinson D, Odille F, et al. Motion corrected compressed sensing for free-breathing dynamic cardiac MRI. Magn Reson Med 2013;70:504–516.
29. Buerger C, Schaeffter T, King AP. Hierarchical adaptive local affine registration for fast and robust respiratory motion estimation. Med Image Anal 2011;15:551–564.
30. Hestenes MR, Stiefel E. Methods of conjugate gradients for solving linear systems. J Res Natl Bureau Stand 1952;49:409–436.
31. Etienne A, Botnar RM, Van Muiswinkel AM, Boesiger P, Manning WJ, Stuber M. "Soap-bubble" visualization and quantitative analysis of 3D coronary magnetic resonance angiograms. Magn Reson Med 2002;48:658–666.
32. Hansen MS, Atkinson D, Sorensen TS. Cartesian SENSE and k-t SENSE reconstruction using commodity graphics hardware. Magn Reson Med 2008;59:463–468.
33. Otazo R, Kim D, Axel L, Sodickson DK. Combination of compressed sensing and parallel imaging for highly accelerated first-pass cardiac perfusion MRI. Magn Reson Med 2010;64: 767–776.